Synthetic Aperture Radar Imaging Using Nonlinear Frequency Modulation Signal

JAMAL SAEEDI
KARIM FAEZ, Member, IEEE
Amirkabir University of Technology
Tehran, Iran

In this paper, a new nonlinear frequency modulation (NLFM) waveform is developed that can be used as a transmitted chirp in synthetic aperture radar (SAR) imaging to improve the imaging quality compared to a linear frequency modulation (LFM) chirp signal. The new NLFM is constructed based on piecewise linear functions, which are optimized using multi-objective optimization. Different signal processing algorithms are investigated in order to use NLFM as the transmitted chirp in a SAR system. In addition, a modified motion compensation (MC) algorithm using navigation data is proposed for the range-Doppler algorithm. Strip-map SAR geometry is considered to generate a SAR raw signal, in order to validate the new offered chirp signal and the proposed MC algorithm.

Manuscript received April 18, 2014; revised September 22, 2014, December 23, 2014, April 6, 2015; released for publication August 3, 2015.

DOI. No. 10.1109/TAES.2015.140310.

Refereeing of this contribution was handled by C. Baker.

Authors' address: Electrical Engineering Department, Amirkabir University of Technology, 424 Hafez Avenue, Tehran, Iran, E-mail: (jamal.saeedi@aut.ac.ir; kfaez@aut.ac.ir).

I. INTRODUCTION

Conventional synthetic aperture radar (SAR) systems use linear frequency modulation (LFM) waveform for imaging. Nonlinear frequency modulation (NLFM) waveform can be used as an alternative in order to get better SAR imaging quality. In this paper, both the linear and nonlinear frequency modulated waveforms are discussed.

Pulse compression is used in radar applications to enhance the range resolution of the radar system without increasing the peak-transmitted power [1]. The most common form of pulse compression waveform is LFM chirp. The matched filter (MF) response of this waveform has a sidelobe level about 13 dB, which can be improved by applying many methods, such as windowing, adaptive filtering [2], and optimization techniques [3]. These techniques can decrease sidelobe levels but at the cost of reduced signal-to-noise ratio (SNR) and a wider main lobe.

Another pulse compression method is NLFM, which can obtain fine resolution and good SNR. It has a spectrum weighting function, which results in a pure MF giving low sidelobes. Therefore, the loss in SNR associated with weighting or with the traditional mismatching methods is eliminated [1]. Amplitude tapering of the transmitted signal is an alternative to NLFM for shaping the spectrum. However, this is not practical since efficient power amplification of the waveform requires the hardware to be operated in a nonlinear way.

A range-compressed signal, or MF profiles, across a series of radar transmissions is the base of SAR signal processing algorithms. Improving SNR and sidelobe levels of range-compressed signal results in better SAR imaging quality. As a result of the current progress in developing digital-to-analog converters and large-scale field programmable gate arrays [4], generating accurate digital NLFM waveforms is not still a problem. Prior reports detailed the design and generation of precision NLFM waveforms [5,6]. The drawback of some NLFM waveforms is its Doppler intolerance. Generally, as Doppler shifts, the MF output value decreases from its peak value. For Doppler-tolerant signals such as a wide bandwidth LFM pulse, a fast Fourier transform (FFT)–based filtering method can be used for matched filtering to simplify receiver complexity. The Doppler intolerance of NLFM waveforms may not be problematic for SAR-related applications. This is because the Doppler bandwidth in SAR is small as compared to the radar applications.

There is no reported real-world application of NLFM waveforms for SAR in the literature. There are some papers that theoretically investigate the usage of a NLFM chirp signal in SAR-related applications. Doerry [7] suggests the usage of NLFM waveform for SAR in a report for Sandia National Laboratories. The focus of the report is the effect of intrapulse Doppler in SAR signal processing. He started with the fact that for NLFM waveforms, the effect of intrapulse Doppler is more

problematic in the signal processing procedure, and it should be considered. The report mainly discusses the significance of the intrapulse Doppler effect on different processing algorithms and ways to compensate for this effect. However, there is no simulation result concerned with using a NLFM waveform in SAR signal processing in this report. Bayindir [8] proposed a new NLFM waveform for SAR imaging and its application to generate synthetic data for testing the change detection methodology and algorithms. However, there is no information in the thesis toward the choice of the new NLFM, and there is no comparison with other alternative NLFM waveforms in terms of sidelobe ratio reduction, resolution, loss in SNR, and Doppler sensitivity.

In this study, a new method based on generalized piecewise linear (PWL) functions is presented to generate a NLFM waveform. Compared to the generally used LFM, this chirp is shown to be capable of reducing the sidelobe levels of the MF response without having an adverse effect on SNR and main-lobe width. Popular methods of NLFM signal generation are investigated, and their performances are assessed by measuring their sidelobe reduction, main-lobe widening, and Doppler sensitivity. The range-Doppler algorithm (RDA) [9], omega-K (ω-K) [10], time domain correlation (TDC), and back-projection (BP) [11] are chosen to investigate the new NLFM chirp signal. In addition, a modified motion compensation (MC) algorithm for the NLFM chirp signal is proposed, which is suitable for the RDA.

The remainder of this paper is organized as follows. Section II gives the description of the new NLFM chirp signal using PWL functions. In section III, signal processing for the NLFM chirp signal is presented. The MC algorithm for a NLFM waveform is explained in section IV. Section V illustrates experimental results. Finally, conclusions are given in section VI.

II. PROPOSED NLFM WAVEFORM

There are many research works that have studied NLFM waveforms and attempted to design the optimum form [12–15]. Generally, there are two NLFM designing procedures. One is based on the principle of stationary phase (PoSP) for shaping the spectrum using a window function [12, 14]. The other one is called the explicit functions cluster method, which requires understanding the modulation rules for various NLFM waveforms [16].

The implementation of spectrum shaping may lead to the penalty of main-lobe widening. In other words, there is no control on the main-lobe requirement. In this study, a NLFM waveform is designed such that its MF response satisfies both the sidelobe and main-lobe requirements together.

A. New NLFM Waveform using PWL Functions

In this study, a new method based on generalized PWL functions is proposed to generate a NLFM waveform. Specifically, an instantaneous frequency function is

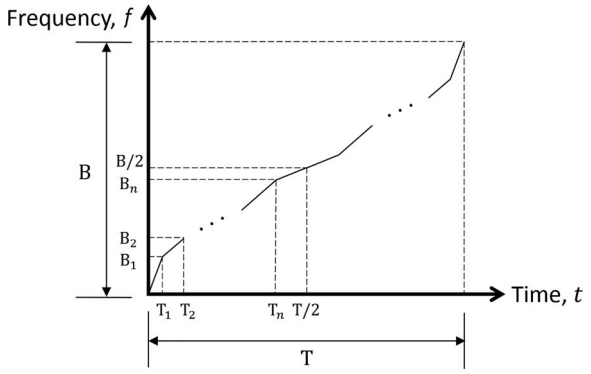

Fig. 1. Frequency modulation signal for $n+1$ stages of PWL functions.

constructed using $n+1$ stages for PWL functions as shown in Fig. 1. Most of the well-known NLFM waveforms [12–16] have the form of the first half reflected; i.e., the second half of the instantaneous frequency is a reflection of the first half. In addition, it is shown through experiments that this kind of transformation leads to better MF results. Therefore, the first-half reflection function is used to generate the second half of the NLFM waveform. The first half of the instantaneous frequency of the proposed NLFM waveform can be formulated as follows:

$$f(t)=\begin{cases} c_0 t & 0\le t<T_1 \\ B_1+c_1(t-T_1) & T_1\le t<T_2 \\ \cdots & \cdots \\ B_n+c_n(t-T_n) & T_n\le t<T/2 \end{cases} \tag{1}$$

where B is the frequency bandwidth, T is the pulse width, and

$$c_0=\frac{B_1}{T_1},\ \underset{1\le m<n}{c_m}=\frac{B_{m+1}-B_m}{T_{m+1}-T_m},\ c_n=\frac{\frac{B}{2}-B_n}{\frac{T}{2}-T_n}$$

and the second half of the proposed NLFM waveform is:

$$f(t)=\begin{cases} B/2+c_n(t-T/2) & T/2\le t<T-T_n \\ B-B_n+c_{n-1}(t+T_n-T) & T-T_n\le t<T-T_{n-1} \\ \cdots & \cdots \\ B-B_1+c_0(t+T_1-T) & T-T_1\le t\le T \end{cases} \tag{2}$$

Then, the phase of this $n+1$ stage NLFM waveform can be derived by integrating (1) and (2) as:

$$\varphi(t)=2\pi\begin{cases} c_0t^2/2+l_0 & 0\le t<T_1 \\ B_1t+c_1\left(t^2/2-T_1t\right)+l_1 & T_1\le t<T_2 \\ \cdots & \cdots \\ B_nt+c_n\left(t^2/2-T_nt\right)+l_n & T_n\le t<T/2 \end{cases} \tag{3}$$

and the phase function for the second half is:

$$\varphi(t) = 2\pi \begin{cases} t \cdot \frac{B}{2} + c_n\left(\frac{t^2}{2} - t \cdot T/2\right) + h_0 & T/2 \le t < T - T_n \\ t \cdot (B - B_n) + c_{n-1}\left(\frac{t^2}{2} + t \cdot (T_n - T)\right) + h_1 & T - T_n \le t < T - T_{n-1} \\ \cdots & \cdots \\ t \cdot (B - B_1) + c_0\left(\frac{t^2}{2} + t \cdot (T_1 - T)\right) + h_n & T - T_1 \le t \le T \end{cases} \tag{4}$$

where $l_0 \ldots l_n$ and $h_0 \ldots h_n$ are used to preserve the continuity between different stages of the phase function. Using simple mathematical operations, these parameters are obtained as:

$$l_0 = 0, l_1 = -\frac{1}{2}B_1T_1 + \frac{1}{2}c_1T_1^2 \tag{5}$$

$$\underset{2\le m\le n}{l_m} = (B_{m-1} - B_m)T_m + \frac{1}{2}T_m^2(c_{m-1} + c_m) - c_{m-1}T_mT_{m-1} + l_{m-1} \tag{6}$$

$$h_0 = -\frac{1}{4}BT + \frac{1}{4}c_nT^2 + \frac{1}{2}B_nT - \frac{c_nT_nT}{2} + l_n \tag{7}$$

$$h_1 = (T - T_n)\left(\left(B_n - \frac{B}{2}\right) + \frac{c_{n-1}}{2}(T - T_n) - \frac{c_nT_n}{2}\right) + h_0 \tag{8}$$

$$\underset{2\le m\le n}{h_m} = (T - T_{n-m+1})\left((B_{n-m+1} - B_{n-m+2}) + \frac{c_{n-m+1}}{2}(T - T_{n-m+1}) - \frac{c_{n-m+2}}{2}(T_{n-m+1} + T - 2T_{n-m+2})\right) + h_{m-1} \tag{9}$$

B. Parameters Selection Based on Multi-Objective Optimization

Having the model to generate the phase function for a NLFM waveform, there are $2n$ parameters ($B_1 \ldots B_n$, and $T_1 \ldots T_n$) to be determined to get the optimum MF response. The following measures are often used to determine the performance of MF response:

1) Sidelobe-to-peak level ratio (SPLR): ratio between the returned signal of the first sidelobe of the MF response and the peak power of main lobe:

$$\text{SPLR} = 10\log\left(\frac{\text{first sidelobe power}}{\text{peak power of main lobe}}\right) \tag{10}$$

2) Integrated sidelobe level ratio (ISLR): ratio between the returned energy of the main lobe and that integrated over several (usually 10 to 20) sidelobes on both sides of the main one:

$$\text{ISLR} = 10\log\left(\frac{\text{power integrated over sidelobes}}{\text{total main lobe power}}\right) \tag{11}$$

3) Impulse response width (IRW): the width of the main lobe of the impulse response, measured 3 dB below the peak value.

In order to find the optimum parameters of the new NLFM waveform, a multi-objective optimization method should be used. One challenge is to use these three objectives at the same time, and the other one is the choice of multi-objective optimizer.

For a convex optimization, all the objective functions and constraints should be convex functions. Note that the objective functions defined by (10), (11), and IRW are not convex over x, and hence, standard convex optimization techniques cannot be used to solve the optimization problem. Global optimization is a branch of applied mathematics that is capable of guaranteeing convergence in finite time to the actual optimal solution of a nonconvex problem. Global optimization is distinguished from regular optimization by its focus on finding the maximum or minimum over all input values, as opposed to finding local minima or maxima.

It is well known that all optimization methods have at least some limitations. There is no single method or algorithm that works the best on all class of problems. Because of the unknown and complicated design space for our nonconvex multi-objective optimization problem, a reliable global optimization algorithm should be used that works for a broad class of optimization problems. Therefore, we have chosen multi-objective goal attainment optimization [17], which is implemented in the MATLAB optimization toolbox. It would be possible to use another multi-objective solver to get better results, but that is beyond the scope of this paper. The goal attainment problem tries to find x to minimize the maximum of:

$$(F_i(x) - G_i)/w_i \tag{12}$$

where x is the parameter that should be estimated, F_i is the objective function, G_i is the goal, w_i is a weight, and i is the index for the objective function.

Generally, this minimization is supposed to be accomplished while satisfying all types of constraints, including:

$$c(x) \le 0, ceq(x) = 0,\ A.x \le b,\ Aeq.x = beq,\ and\ l \le x \le u$$

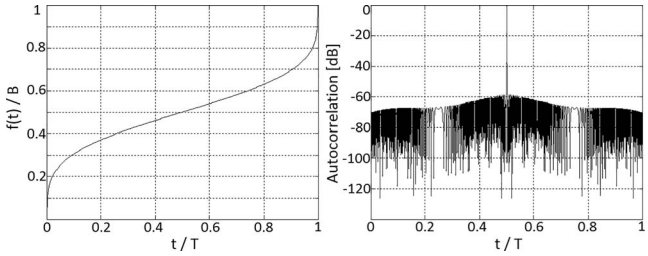

Fig. 2. Proposed NLFM waveform using 64 parameters ($n = 32$) (left), and MF output (right).

where the matrix A and vector b are, respectively, the coefficients of the linear inequality constraints and the corresponding right-side vector. The matrix Aeq and vector beq are, respectively, the coefficients of the linear equality constraints and the corresponding right-side vector. Here, x is the solution found by the optimization function, l and u are lower and upper bound vectors of the solution space, $c(x)$ is the function that computes the nonlinear inequality constraint, and $ceq(x)$ computes the nonlinear equality constraint.

In other words, the goal attainment problem is to minimize a slack variable γ, defined as the maximum over i of the expressions (12). This suggests an expression representing the formal statement of the goal attainment problem:

$$\begin{aligned} &\min_{x,\,\gamma} \gamma, \text{ such that } F(x) - w \cdot \gamma \le G, \quad c(x) \le 0, \\ &ceq(x) = 0, \ A \cdot x \le b, \ Aeq \cdot x = beq, \\ &and\ l \le x \le u \end{aligned} \tag{13}$$

The term $w \cdot \gamma$ introduces an element of slackness into the problem, which otherwise forces the optimization algorithm to strictly satisfy the goals. The weighting vector w allows the relative compromises between the objectives. The preceding details have been implemented in the "fgoalattain" function of the MATLAB optimization toolbox. Here, we have used SPLR(x) and ISLR(x) as two objectives (F_1 and F_2), and IRW(x) is used in the nonlinear inequality constraint $c(x) \le 0$, where $c(x) = \text{IRW}(x) - v \cdot \text{IRW}_{\text{LFM}} \cdot \text{IRW}_{\text{LFM}}$ is the impulse response width of the MF in the LFM waveform case, and v is a widening factor, which is chosen in order to control the IRW in the optimization procedure, and we set it to 1.35. To get better SPLR and ISLR in the MF response, this parameter can be increased. In addition, G_1 and G_2 are set to $\{-40, \ -65\}$, and the weights w_1 and w_2 are $\{1, 2\}$, which are obtained through experiments. In general, some form of trial-and-error tuning is necessary for each particular instance of the optimization problem. The widening factor v, G_1, G_2, and the weights can be changed based on the system requirements, including IRW, SPLR, and ISLR of the MF response.

The overall shape of frequency modulation and pulse-compressed response of the proposed waveform is shown in Fig. 2. Complete discussions and comparisons with other NLFM waveforms are given in the results section.

III. SIGNAL PROCESSING FOR NLFM CHIRP SIGNAL

In this section, first we will describe how to model the transmitted and received signal based on the NLFM waveform. Then, different time and frequency domain algorithms for image formation of the received SAR signal are explained.

Before the SAR signal is generated, a number of important system parameters should be determined, including carrier frequency, bandwidth, pulse length, and pulse repetition frequency (PRF). The transmitted signal is a NLFM waveform, where the signal spans the bandwidth over the pulse length. This cycle is repeated at the PRF. The SAR signal is usually generated at or near baseband and then mixed up to the desired operating frequency before transmission. The NLFM transmit signal can be expressed as:

$$s_t(t) = A(t) \exp\left(j\left(2\pi f_0 t + \varphi(t) + \varphi_0\right)\right) \tag{14}$$

where $A(t)$ is the signal amplitude and defines the pulse length with a Rect function, $\varphi(t)$ is the phase function expressed in (3) and (4), f_0 is the frequency at the beginning of the chirp, and φ_0 is the starting phase, which can usually be neglected.

A power amplifier increases the signal power to a specified level in the transmission chain. An antenna propagates the amplified signal to the target area. A very small portion of the transmitted signal is reflected back to the radar. The echoed signal from teh target can be expressed as:

$$\begin{aligned} s_r(t, \eta) = A'(t) \exp(j(2\pi f_0 (t - \tau) \\ + \varphi(t - \tau) + \varphi_0)) \end{aligned} \tag{15}$$

where t is the fast time, η is the slow time (or azimuth time), $A'(t)$ is an attenuated version of $A(t)$, and τ is the two-way time of flight to the target at range R.

The received signal is amplified with a low-noise amplifier (LNA) and mixed down to an appropriate band for sampling. After the signal from (15) is mixed down by a frequency f_m, the signal ready to be recorded is:

$$\begin{aligned} s_{rm}(t, \eta) = A''(t) \exp(j(2\pi f_0 (t - \tau) + \varphi(t - \tau) \\ + \varphi_0 - 2\pi f_m t)) \end{aligned} \tag{16}$$

where $A''(t)$ is an amplified version of $A'(t)$.

For simplification, let $f_m = f_0$; therefore,

$$s_{rm}(t, \eta) = A''(t) \exp\left(j\left(-2\pi f_0 \tau + \varphi(t - \tau) + \varphi_0\right)\right) \tag{17}$$

SAR systems digitize this data set and either store it on board, transmit it to a ground station, or process it onboard. In the following, different time and frequency domain algorithms for processing raw data based on a NLFM waveform as the transmitted signal will be described.

A. Time Domain Correlation

The TDC algorithm uses the raw data directly, without range compression. In this case, a SAR image from a point target is formed using the following formula:

$$im(x_0, y_0, z_0) = \sum_t \sum_\eta s_{rm}(t, \eta) \exp\left(j\Phi_{\tau_0}(t, \eta)\right) \quad (18)$$

where (x_0, y_0, z_0) is the coordinate of the point target, Φ_{τ_0} is negative of the phase in (17), which can be expressed as:

$$\Phi_{\tau_0}(t, \eta) = -(-2\pi f_0 \tau_0 + \varphi(t - \tau_0) + \varphi_0) \quad (19)$$

and τ_0 is obtained using the following:

$$\tau_0(t, \eta) = \frac{2R(t, \eta)}{c} = \frac{2\sqrt{(H - z_0)^2 + y_0^2 + (v(t + \eta) - x_0)^2}}{c} \quad (20)$$

where v is the platform velocity, H is the flight altitude, and c is the speed of light.

This is a very exact method, but it is very computationally taxing, and so it is rarely used in practice. However, it is important, because it gives a reference for measuring the imaging quality of other reconstruction algorithms.

B. Back-Projection

The BP algorithm normally operates on range-compressed data [11]. For SAR data, range compression can be performed using MF. Using the stop and go approximation, τ_0 does not depend on fast time t, and we can rewrite (18) as

$$im(x_0, y_0, z_0) = \sum_\eta \exp(j2\pi f_0 \tau_0) \sum_t s_{rm}(t, \eta) \times \exp(-j\varphi(t - \tau_0)) \quad (21)$$

The inner sigma in (21) is the definition of MF. For range compression, we define a reference chirp equal to the transmit signal. When the received signal is convolved with the reference chirp, the result is a peak where the signals line up. This peak corresponds to the target range. In processing, this is efficiently done with a FFT, a complex-phase multiplication, and an inverse FFT.

$$s_{rc}(\tau_0, \eta) = \sum_t s_{rm}(t, \eta) \exp(-j\varphi(t - \tau_0)) \approx a\mathrm{Sinc}(b(t - \tau_0)) \quad (22)$$

where a and b are constants. Using (22), (21) can be reformulated as:

$$im(x_0, y_0, z_0) = \sum_\eta \exp(j2\pi f_0 \tau_0) s_{rc}(\tau_0, \eta) \quad (23)$$

The benefits of BP include the simplicity of the algorithm, the parallel computation structure, and the ability to process data from an arbitrary platform path. Similar to the TDC method, the motion of the platform must be precisely known for the BP algorithm.

C. Omega-K Algorithm

The Omega-K algorithm [10] works on the wave-number or two-dimensional (2-D) frequency domain of the SAR signal, which is based on a LFM waveform. In order to derive the algorithm for a NLFM chirp signal, some modifications should be done. First, a FFT is performed to transform the SAR signal data into the range frequency domain:

$$\begin{aligned} S_{rm}(f_r, \eta) = \mathcal{F}_t\{s_{rm}(t, \eta)\} &= A \cdot \mathrm{B}(\mathrm{f_r}) \cdot \exp(-j2\pi f_0 \tau) \\ &\cdot \mathcal{F}_t\{\exp(j\varphi(t - \tau))\} = A \cdot \mathrm{B}(f_r) \\ &\cdot \exp(-j2\pi f_0 \tau) \cdot \exp(-j2\pi f_r \tau) \\ &\cdot \mathcal{F}_t\{\exp(j\varphi(t))\} \end{aligned} \quad (24)$$

where A is a constant, and $B(f_r)$ is a complex function that limits the values of S_{rm} to within the bandwidth of the chirp. $B(f_r)$ can be approximated by a Rect function.

For a NLFM chirp signal, $\mathcal{F}_t\{\exp(j\varphi(t))\}$ cannot be easily expressed, unlike the LFM waveform. Therefore, we should eliminate this expression in (24) in order to obtain the SAR signal formula in the 2-D frequency domain. To aim this, we obtain the Fourier transform of the time-reversed conjugate of the reference chirp as:

$$H_r(f_r, \eta) = A' \cdot B'(f_r) \cdot \mathcal{F}_t\{\exp(-j\varphi(-t))\} \quad (25)$$

where A' is a constant, and $B'(f_r)$ is a complex function, which can be approximated by a Rect function.

Then, (24) and (25) are multiplied together,

$$\begin{aligned} S_r(f_r, \eta) &= H_r(f_r, \eta) \times S_{rm}(f_r, \eta) \\ &\approx A'' \cdot \mathrm{B}''(\mathrm{f_r}) \cdot \exp(-j2\pi(f_0 + f_r)\tau) \end{aligned} \quad (26)$$

where A'' is a constant, and $B''(f_r)$ is approximately the same as $B'(f_r)$.

We now expand the time delay τ in (26) to the range to target $R(\eta)$. The phase function after the range Fourier transform is obtained as:

$$\phi_r(f_r, \eta) = -4\pi(f_0 + f_r) \cdot R(\eta)/c \quad (27)$$

where $R(\eta) = \sqrt{r_0^2 + (v \cdot \eta - x_0)^2}$, and r_0 is the closest approach from platform to the target, $r_0 = \sqrt{H^2 + y_0^2}$.

We can approximate the azimuth Fourier transform using the PoSP. An expression for the signal phase in the azimuth Fourier transform integral is computed by adding the phase term $-2\pi f_a \eta$ to (27), where f_a is the azimuth frequency.

$$\phi = -4\pi(f_0 + f_r) \cdot R(\eta)/c - 2\pi f_a \eta \quad (28)$$

We then take the derivative of the phase with respect to η, and solve it for η at the point where the phase is stationary (i.e., where $d\phi/d\eta = 0$). We substitute the obtained η into (28) and simplify it to obtain the signal phase after the azimuth Fourier transform of the signal. The exponential, which makes up the signal in the 2-D

frequency domain, can be expressed as:

$$S_r(f_r, f_a) = \exp\left(-j\left(\frac{2\pi r_0}{v \cdot c}\sqrt{4(f_0+f_r)^2 \cdot v^2 - f_a^2 c^2} + \frac{2\pi \cdot f_a x_0}{v}\right)\right) \tag{29}$$

Then, the reference function multiplication (RFM) is applied [18]. The reference function is computed for a reference range r_{ref}. A target at the reference range is correctly focused by the RFM, but targets away from that range are only partially focused. The RFM filter can be expressed as:

$$\mathrm{RFM}\left(f_r, f_a, r_{ref}\right) = \exp\left(j\frac{2\pi r_{ref}}{v \cdot c}\sqrt{4(f_0+f_r)^2 \cdot v^2 - f_a^2 c^2}\right) \tag{30}$$

where r_{ref} denotes the reference range, which is generally defined as the closest slant range from the scene center to the receiver.

The next step is the Stolt interpolation [19]. This completes the focusing of targets away from the reference range r_{ref} by remapping the range frequency axis. Finally, a 2-D inverse FFT is performed to transform the data back to the time domain, i.e., the SAR image domain (as the inverse FFT of a sine wave is a Sinc function):

$$im(t, \eta) = p_r\left(t - \frac{2\left(r_0 - r_{ref}\right)}{c}\right) \cdot p_a\left(\eta - \frac{x_0}{v}\right) \tag{31}$$

where $p_r(t)$ and $p_a(\eta)$ are the compressed pulse envelope in the range and the azimuth directions, respectively.

D. Range-Doppler Algorithm

The most frequently used algorithm for SAR signal processing is the range-Doppler algorithm (RDA) [9]. In order to use the RDA for processing the raw signal based on a NLFM chirp signal, we rewrite (29) as:

$$S_r(f_r, f_a) = \exp\left(-j\left(\frac{4\pi r_0 f_0}{c}\sqrt{D^2(f_a) + \frac{2f_r}{f_0} + \left(\frac{f_r}{f_0}\right)^2} + \frac{2\pi \cdot f_a x_0}{v}\right)\right) \tag{32}$$

where

$$D(f_a) = \sqrt{1 - \left(\frac{c f_a}{2v f_0}\right)^2}$$

The RDA is obtained as a result of using Taylor series approximation of (32). The square root term in (32) can be expanded as:

$$\Gamma(f_r) = \sqrt{D^2(f_a) + \frac{2f_r}{f_0} + \left(\frac{f_r}{f_0}\right)^2} \approx \Gamma(0) + \frac{\Gamma'(0)}{1!}f_r + \frac{\Gamma''(0)}{2!}f_r^2 + \cdots \tag{33}$$

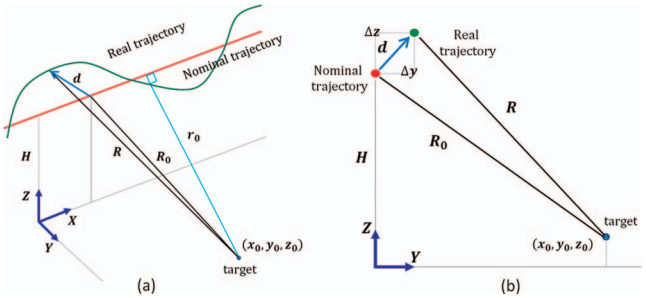

Fig. 3. (a) SAR geometry, and (b) normal plane of ideal trajectory.

The RDA keeps only up to the first order,

$$\Phi_{\mathrm{RDA}} = -\left(\frac{4\pi r_0 f_0}{c} \cdot \left[D(f_a) + \frac{f_r}{f_0 . D(f_a)}\right] + \frac{2\pi . f_a x_0}{v}\right) \tag{34}$$

which makes the algorithm relatively simple. Using this approximation, the inverse Fourier transform of (32) in the range direction gives us the signal in the range-Doppler domain:

$$S_r(\tau, f_a) \approx p_r\left(\tau - \frac{2r_0}{c.D(f_a)}\right) \cdot \exp\left(-j\left(\frac{4\pi r_0 f_0}{c} \cdot D(f_a) + \frac{2\pi \cdot f_a x_0}{v}\right)\right) \tag{35}$$

With the SAR signal range-compressed and the range cell migration removed, the signal can be expressed in the range-Doppler domain as:

$$S_r(\tau, f_a) \approx p_r\left(\tau - \frac{2r_0}{c}\right) \cdot \exp\left(-j\left(\frac{4\pi r_0 f_0}{c} \cdot D(f_a) + \frac{2\pi \cdot f_a x_0}{v}\right)\right) \tag{36}$$

After azimuth matched filtering, an inverse azimuth FFT returns the signal to the time domain, where the targets are now fully compressed:

$$im(\tau, \eta) = p_r\left(\tau - \frac{2r_0}{c}\right) \cdot p_a\left(\eta - \frac{x_0}{v}\right) \tag{37}$$

IV. MOTION COMPENSATION ALGORITHM FOR NLFM CHIRP SIGNAL

The SAR processing algorithms described in section III assume that the platform moves at a constant speed in a straight line. Translational motion causes a platform displacement from the nominal, ideal path as shown in Fig. 3a. This results in the target scene changing in range during data collection. This range shift also causes inconsistencies in the target phase history. A target at range R_0 measured at range $R = R_0 + \Delta R_0$ results in a phase error in (17):

$$s_{\Delta rm}(t, \eta) = A''(\mathrm{t}) \cdot \exp(j(-2\pi f_0(\tau_0 + \Delta\tau_0) + \varphi(t - (\tau_0 + \Delta\tau_0)) + \varphi_0)) \tag{38}$$

where $\tau_0 = 2R_0/c$, $\Delta\tau_0 = 2\Delta R_0/c$, ΔR_0 is small deviation from R_0 due to nonlinear motion, $\Delta R_0 = R - R_0$ (see Fig. 3), and φ_0 is the starting phase, which is unknown and will be neglected in the remaining discussion.

Unlike for the LFM case, the phase error in (38) cannot be simply expressed in the time domain for a NLFM chirp signal. Fortunately, if the motion is known (using an onboard inertial navigation system/global positioning system (INS/GPS) sensor), then the motion errors can be compensated. Here, the strip-map SAR geometry of Fig. 3a is assumed. The instantaneous motion error vector d, defined by the displacement between the real and nominal trajectories, is $[\Delta x(\eta), \Delta y(\eta), \Delta z(\eta)]$, where $\Delta y(\eta)$ and $\Delta z(\eta)$ represent the cross-track displacement as shown in Fig. 3b. Knowing the coordinates of target (x_0, y_0, z_0), the real trajectory, and the nominal trajectory, the distances R and R_0 can be calculated from geometry:

$$\begin{aligned} &R(\eta; x_0, y_0, z_0) \\ &= \sqrt{(v\cdot\eta+\Delta x(\eta)-x_0)^2+(\Delta y(\eta)-y_0)^2+(H+\Delta z(\eta)-z_0)^2} \\ &= R_0(\eta; x_0, y_0, z_0) + \Delta R_0(\eta; x_0, y_0, z_0) \end{aligned} \tag{39}$$

$$R_0(\eta; x_0, y_0, z_0) = \sqrt{(v.\eta - x_0)^2 + y_0^2 + (H - z_0)^2} \tag{40}$$

The traditional MC method for RDA involves two steps. First, the corrections are calculated for a reference range, R_{ref}, usually in the center of the swath. The first step of phase correction is as:

$$H_{mc_1} = \exp\left(j2\pi f_0 \Delta\tau_{ref}\right) \tag{41}$$

where $\Delta\tau_{\text{ref}} = 2\Delta R_{\text{ref}}/c$, and $\Delta R_{\text{ref}} = R - R_{\text{ref}}$ (and distances R and R_{ref} are calculated from real and nominal trajectories, respectively, to a target in the center of the swath). Then, the SAR data are range-compressed. This is the center-beam approximation [20] and is used in many MC algorithms. A second-order correction is applied to each range, according to the differential correction from the reference range. For each R, ΔR_0 is calculated, and the correction is formed as:

$$H_{mc_2} = \exp\left(j2\pi f_0\left(\Delta\tau_0 - \Delta\tau_{ref}\right)\right) \tag{42}$$

This method introduces error after the range compression, which is not acceptable for a high-resolution SAR system. In this study, an efficient MC method is proposed to apply to the range-compressed data. The range-compressed signal of (38) can be obtained using matched filtering as follows:

$$\begin{aligned} s_{\Delta rc}(\tau,\eta) &= \mathcal{F}^{-1}{}_{f_r}\{\mathcal{F}_t\{s_{\Delta rm}(t,\eta)\}\cdot\mathcal{F}_t\{\exp(-j\varphi(-t))\}\} \\ &= \mathcal{F}^{-1}{}_{f_r}\{A.\mathrm{B}(f_r)\cdot\exp(-j2\pi(f_0+f_r)(\tau_0+\Delta\tau_0)) \\ &\quad\cdot\mathcal{F}_t\{\exp(j\varphi(t))\}\cdot\mathcal{F}_t\{\exp(-j\varphi(-t))\}\} \\ &= \mathcal{F}^{-1}{}_{f_r}\{A.\mathrm{B}(f_r)\cdot\exp(-j2\pi f_r(\tau_0+\Delta\tau_0)) \\ &\quad\cdot\mathcal{F}_t\{\exp(j\varphi(t))\}\cdot\mathcal{F}_t\{\exp(-j\varphi(-t))\}\} \\ &\quad\cdot\exp(-j2\pi f_0(\tau_0+\Delta\tau_0)) \\ &\approx p_r(\tau-(\tau_0+\Delta\tau_0))\cdot\exp(-j2\pi f_0(\tau_0+\Delta\tau_0)) \end{aligned} \tag{43}$$

TABLE I
Key Simulation Parameters

Parameter	Value
Pulse width (μs)	13
Bandwidth (MHz)	100
Sampling frequency (MHz)	360

TABLE II
Results of Pulse Compression of Different NLFM Waveforms

Frequency Modulation	SPLR_{dB}	ISLR_{dB}	$\text{IRW}_{\text{sample}}$
LFM	−13.38	−4.11	3.54
Cosine, $n = 1$ [12]	−22.98	−18.71	4.25
Cosine, $n = 2$	−29.78	−18.00	5.17
Tangent-based [13]			
$\alpha = 5$	−32.27	−30.04	6.09
$\alpha = 6$	−36.40	−33.76	6.71
Truncated Gaussian [14]			
$k = 50$	−31.53	−13.47	5.12
$k = 90$	−35.25	−13.78	6.73
Hybrid NLFM [15]	−38.41	−37.58	6.21
Proposed NLFM			
$v = 1.25$	−38.34	−34.25	4.45
$v = 1.35$	−47.36	−37.50	4.81
$v = 1.60$	−59.01	−39.84	5.70

where $\mathcal{F}_t\{s_{\Delta rm}(t,\eta)\}$ is obtained using (24), A is a constant, $B(f_r)$ is a complex function that limits the values of $\mathcal{F}_t\{s_{\Delta rm}(t,\eta)\}$ to within the bandwidth of the chirp [and $B(f_r)$ can be approximated by a Rect function], and $p_r(\tau)$ is the compressed pulse envelope in the range direction. The simplification that gives the last line of (43) is due to the fact that the multiplication in the frequency domain corresponds to convolution in the time domain. Therefore, the compressed pulse envelope $p_r(\tau)$ is the result of the NLFM signal autocorrelation.

From (43), we can find a correction filter, which works on the range-compressed data as:

$$H(\tau,\eta) = \exp(j2\pi f_0\Delta\tau_0) \tag{44}$$

After the filtering, the range-compressed data becomes:

$$s_{\Delta rc}(\tau,\eta) \approx p_r(\tau-(\tau_0+\Delta\tau_0))\exp(-j2\pi f_0\tau_0) \tag{45}$$

For exactly removing phase error from data, an azimuth-dependent interpolation should be used to compensate the range shift due to motion error:

$$s_{rc}(\tau,\eta) \approx p_r(\tau-\tau_0)\exp(-j2\pi f_0\tau_0) \tag{46}$$

V. EXPERIMENTAL RESULTS

In this section, first we will compare the proposed NLFM chirp signal with other well-known NLFM waveforms, which are designed based on spectrum shaping method [12–15]. Three different measures, including SPLR, ISLR, and IRW, are used to determine the performance of different waveforms. The simulation parameters are given in Table I, and the simulation results of different waveforms are illustrated in Table II. It can be

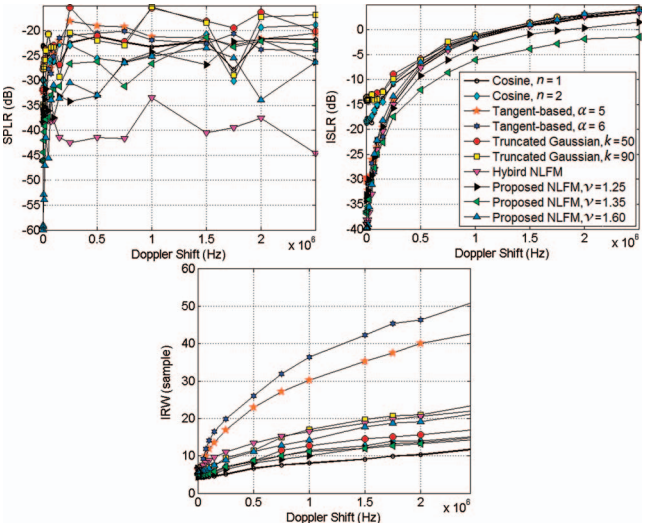

Fig. 4. Doppler sensitivity results of different NLFM waveforms, from top left clockwise: SPLR, ISLR, and IRW of pulse compression results versus Doppler shift.

TABLE III
SAR System Parameters for Raw Data Simulation

Parameter	Value	Parameter	Value
Velocity (m/s)	60	Carrier frequency (GHz)	9
Bandwidth (MHz)	100	Sampling frequency (MHz)	220
Pulse width (μs)	35	Flight time (s)	8
Swath width (m)	700	Minimum range (m)	4663
PRF (Hz)	300	Maximum range (m)	5361
Altitude (m)	5000	Signal-to-noise ratio (dB)	-45
Incident angle (deg)	45	Azimuth beamwidth (deg)	4

seen from the results that the proposed NLFM represents a better compromise among SPLR, ISLR, and IRW indexes as compared to other alternative waveforms. In addition, different NLFM waveforms are investigated based on Doppler sensitivity. The performance of different waveforms versus Doppler shift is depicted in Fig. 4. It can be observed from the results that the proposed NLFM waveform has better tolerance against Doppler shift for the IRW measure; however, for the ISLR and SPLR indexes, the behaviors of different waveforms are almost similar as Doppler shifts.

In order to validate the new offered chirp signal, strip-map SAR imaging geometry together with different reconstruction algorithms derived in section III are considered. The synthetic examples are generated for both point and distributed targets, and it is shown that a NLFM chirp can improve imaging quality compared to a LFM chirp. The simulation parameters for the SAR system are given in Table III. The raw signal for a point target is obtained using the model described in (17). To generate a raw signal from a real SAR image (which is composed of digital complex-valued samples), the SAR image should be resampled (or interpolated) based on the simulation parameters, including the swath width, flight time, range, and azimuth resolutions. After resampling, each sample in the image should represent a resolution cell on the ground for the SAR echo simulation. Then, delay time τ should be obtained for each point target or image sample using the SAR imaging geometry, and the raw signal is obtained using the model described in (17). Finally, all of the raw signals for image samples are weighted and summed with their corresponding amplitudes in the resampled SAR image.

After generating the SAR raw signal, RF noise is added to it (RF noise is simulated through filtering the Gaussian noise). It should be mentioned that because of the randomness property of noise, RF noise is generated once, and it is used similarly for different experiments. The results of point target analysis are obtained for three different scenarios including LFM waveform, LFM + windowing, and NLFM waveform. A Taylor window is typically used in radar applications, such as weighting SAR images and antenna design. Therefore, we have chosen the Taylor window for sidelobe reduction of the MF response. The Taylor window parameter is chosen to have an approximately the same result compared to the NLFM waveform in a noise-free condition.

Four different measures, including SPLR, ISLR, IRW, and 2-D ISLR, are used to evaluate the performance of different algorithms in different scenarios. The 2-D ISLR is similar to the one-dimensional (1-D) ISLR, with the main lobe defined within a rectangle with the size of the respective IRWs in each direction multiplied by a constant (10 or more). The sidelobe power is then the power of the entire 2-D image minus the main-lobe power [18].

The results of different algorithms for point target analysis are shown in Tables IV and V. It can be seen that time domain algorithms (Table IV) have better performances compared to the frequency domain methods (Table V). The results for the NLFM waveform in both time and frequency domain algorithms show improvements compared to the LFM waveform and LFM + windowing scenarios. Because of the mismatch condition between the transmitted and received waveform in the LFM + windowing scenario, both the SNR and the resolution are weaker as compared to the NLFM waveform case. Sidelobe reduction results in main-lobe widening of the MF response in LFM + windowing and NLFM waveform scenarios as compared to the LFM waveform case. However, it is an essential stage in radar imaging to get an image with high contrast. Therefore, it is advisable to use a NLFM waveform for this purpose.

For better clarification, reconstructed image contours of time and frequency domain algorithms in different scenarios for multiple point scatterers are shown in Figs. 5 and 6, respectively. It should be mentioned that the objective results shown in Tables IV and V are related to the point target in the center. The reconstructed image contours are given on a decibel scale. In a good reconstructed image, the point targets should be well separated. This needs an image with high SNR and low sidelobe levels. In the results, a contour image with darker (bluer) regions around the point targets has better SNR

TABLE IV
Results of Point Target Analysis, for the Time Domain Signal Processing Algorithms

Method	TDC (LFM)	TDC (LFM + Windowing)	TDC (NLFM)	BP (LFM)	BP (LFM + Windowing)	BP (NLFM)
$SPLR_{dB}$						
Ground range	−21.88	−28.39	−30.25	−15.90	−27.03	−29.81
Azimuth	−29.61	−28.21	−33.54	−20.88	−21.63	−27.59
$ISLR_{dB}$						
Ground range	−10.95	−13.32	−13.31	−4.74	−9.35	−10.24
Azimuth	−12.28	−12.54	−12.58	−6.10	−5.97	−9.27
2D $ISLR_{dB}$	−6.28	−5.63	−6.88	−4.95	−4.42	−5.86
IRW_{sample}*						
Ground range	1.12	1.74	1.69	1.52	1.93	1.78
Azimuth	0.73	0.74	0.73	0.74	0.73	0.72

*Each sample in azimuth direction is equal to 0.25 m, and in ground range direction is 1.5 m.

TABLE V
Results of Point Target Analysis, for the Frequency Domain Signal Processing Algorithms

Method	RDA (LFM)	RDA (LFM + Windowing)	RDA (NLFM)	ω-k (LFM)	ω-k (LFM + Windowing)	ω-k (NLFM)
$SPLR_{dB}$						
Slant range	−15.70	−28.99	−32.06	−16.20	−28.71	−29.55
Azimuth	−23.22	−19.04	−22.46	−23.57	−23.72	−23.91
$ISLR_{dB}$						
Slant range	−4.93	−9.04	−8.71	−5.54	−9.23	−9.67
Azimuth	−12.50	−9.73	−13.35	−13.75	−13.54	−14.54
2D $ISLR_{dB}$	−1.77	−1.24	−2.64	−2.09	−0.42	−2.697
IRW_{sample}*						
Slant range	2.09	2.89	2.87	2.010	2.83	2.81
Azimuth	1.13	1.13	1.13	1.11	1.11	1.11

*Each sample in azimuth direction is equal to 0.22 m, and in slant range direction is 0.69 m.

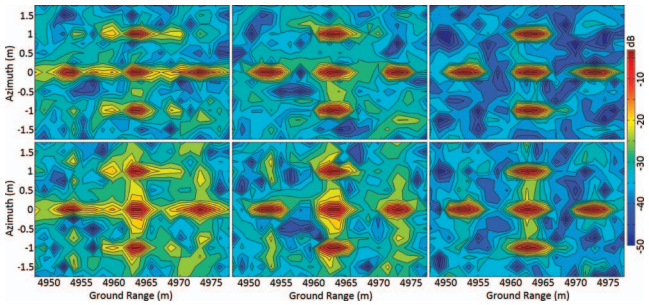

Fig. 5. Comparison of different time domain algorithms in different scenarios. Top row, left to right: TDC results with LFM, LFM + windowing, and NLFM; bottom row: BP algorithm results.

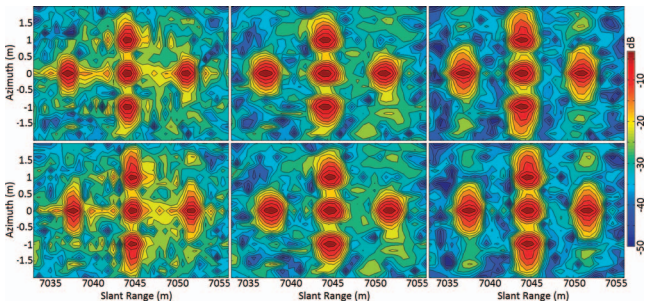

Fig. 6. Comparison of different frequency domain algorithms in different scenarios. Top row, left to right: RDA results with LFM, LFM + windowing, and NLFM. bottom row: omega-K algorithm results.

and lower sidelobe levels. It can be seen from the results that the improvement when using a NLFM waveform is superior for the TDC method compared to the BP algorithm. This is because the TDC algorithm is a very exact method without any approximation. As we have discussed in section III, the BP algorithm uses start and stop approximation in order to range compress SAR data via MF.

It can also be seen from the results that the time domain algorithms have better performance compared to the frequency domain methods (this is because of the approximations used in deriving the frequency domain algorithms, which are discussed in section III). It should be mentioned that the results for RDA and omega-K algorithms are obtained in the slant range-azimuth surface (to obtain the image in the ground-range azimuth surface, a 1-D interpolation should be used).

We perform another experiment in order to show the performances of the different NLFM waveforms in SAR scenarios. Since the matching condition is provided between the transmitted and the received signals for NLFM waveforms, there is no loss in SNR after matched filtering. Therefore, for better demonstration of the improvement using the proposed NLFM waveform, the simulation is performed in a noise-free condition. The SAR system parameters shown in Table III are used for this simulation. It should be mentioned that the parameters

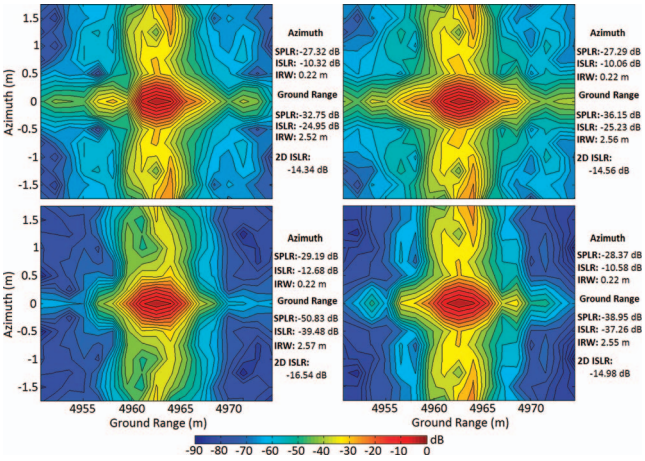

Fig. 7. Comparison of different NLFM waveforms used in SAR scenario with point target. From top left, clockwise: Cosine, $n = 1$ [12], tangent-based [13], hybrid NLFM [15], and the proposed NLFM.

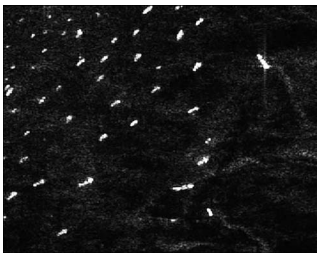

Fig. 8. Real sar image used to simulate raw data (this SAR image shows area of sea near busy port).

of different NLFM waveforms are selected based on having approximately the same resolution in the range direction. Fig. 7 shows the point target response reconstructed using the BP algorithm for different waveforms, which are used in the raw data simulation. It can be seen from the results that the proposed NLFM waveform has better sidelobe reduction with approximately the same resolution as compared to the traditional NLFM waveforms.

We have also performed an experiment to simulate a raw signal based on a NLFM chirp signal for a distributed target. Fig. 8 shows a real SAR image that is used as input for raw signal simulation. The SAR system parameters shown in Table III are used for this simulation. Reconstructed images using different signal processing algorithms derived for NLFM signals are shown in Fig. 9. From the results, it can be seen that the SNR and resolution are better for time domain algorithms as compared to the frequency domain algorithms.

For a final experiment, real flight GPS data are used to generate a SAR raw signal for both point and distributed targets to validate the proposed MC algorithm for a NLFM waveform. It should be mentioned that for better demonstration of the improvement using the proposed MC algorithm, the simulations are performed in a noise-free condition. The results of traditional and proposed MC algorithms are shown in Figs. 10 and 11 for point and

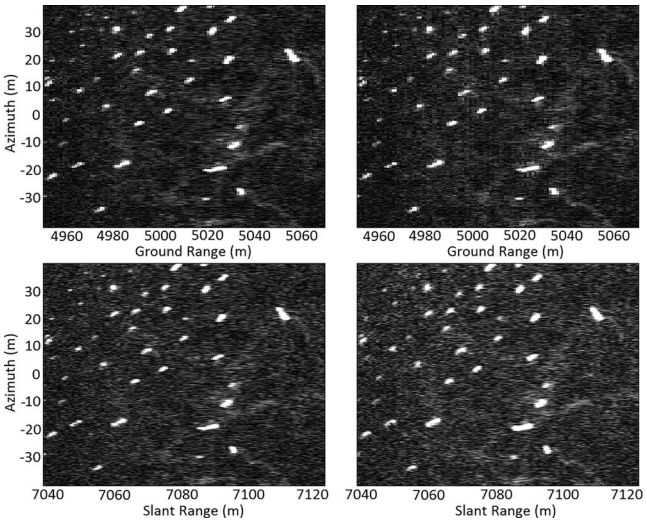

Fig. 9. Results of distributed target analysis, from top left, clockwise: TDC, BP, RDA, and omega-K algorithms.

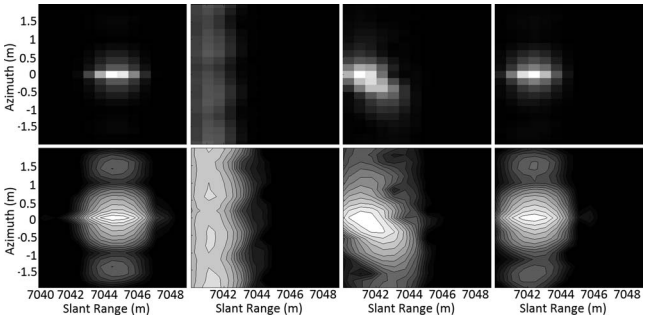

Fig. 10. MC results. Top row, left to right: Amplitude image obtained in ideal case, without MC, traditional MC [20], and proposed MC. Bottom row: contour image of logarithmic scale for better visual comparison.

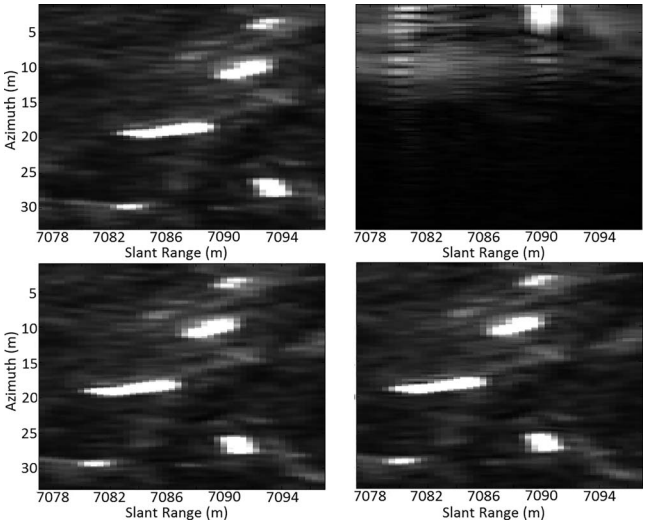

Fig. 11. MC results. From top left, clockwise: Amplitude image obtained in ideal case, without MC, traditional MC [20], and proposed MC.

distributed targets, respectively. In addition, the objective results of point target analysis are shown in Table VI. For the point target analysis shown in Fig. 10, it can be

TABLE VI
Results of MC Experiment for Point Target

Method	Ideal Case	Traditional [20]	Proposed
$SPLR_{dB}$			
Slant range	−41.136	−32.570	−35.127
Azimuth	−23.726	−27.296	−23.766
$ISLR_{dB}$			
Slant range	−28.370	−21.038	21.722
Azimuth	−14.888	−14.960	−14.435
2D $ISLR_{dB}$	−19.699	−9.858	−9.879
IRW_{sample}*			
Slant range	2.850	2.740	2.880
Azimuth	1.090	2.420	1.390

*Each sample in azimuth direction is 0.22 m, and in range direction is 0.69 m.

visually observed that the proposed algorithm outperforms the traditional MC method in terms of resolution, sidelobe levels, and accuracy of target location. In addition, from the numerical results in Table VI, we can see that the azimuth resolution of the point target obtained by the proposed method is 1.32 samples; however, the azimuth resolution is 2.42 samples for the traditional MC method. Therefore, the objective measures SPLR, ISLR, and IRW should be considered all together for justification. For the distributed target analysis shown in Fig. 11, there are improvements in terms of resolution and accuracy of target location for the proposed method.

VI. CONCLUSIONS

In this paper, a new NLFM waveform is proposed that can be used as a transmitted chirp in SAR imaging to improve the imaging quality compared to a LFM chirp signal. Time domain signal processing algorithms (TDC and BP) and frequency domain methods (RDA and omega-K) are modified in order to use the NLFM waveform as the transmitted chirp for SAR imaging. In addition, a modified MC algorithm is developed for phase error compensation in the NLFM waveform case. Experimental results demonstrate effectiveness of the proposed NLFM waveform and the new MC algorithm in terms of SAR image quality metrics.

REFERENCES

[1] Skolnik, M. I.
Radar Handbook (3rd ed.). New York: McGraw-Hill, 2008.

[2] Ackroyd, M. H., and Ghani, F.
Optimum mismatched filters for sidelobe suppression.
IEEE Transactions on Aerospace and Electronic Systems, **AES-9**, 2 (1973), 214–218.

[3] DeGraaf, S. R.,
Sidelobe reduction via adaptive FIR filtering in SAR imagery.
IEEE Transactions on Image Processing, **3**, 3 (1994), 292–301.

[4] Jeong, H., Park, J. H., Ryu, H. Y., Kwon, J. B., and Oh, Y.
VLSI architecture for SAR data compression.
IEEE Transactions on Aerospace and Electronic Systems, **38**, 2 (2002), 427–440.

[5] Doerry, W.
Generating nonlinear FM chirp waveforms for radar.
Sandia National Laboratories, Albuquerque, NM, Sandia Report SAND2006-5856, Unlimited Release, 2006.

[6] Fowle, E.
The design of FM pulse compression signals.
IEEE Transactions on Information Theory, **10**, 1 (1964), 61–67.

[7] Doerry, W.
SAR processing with non-linear FM chirp waveforms.
Sandia National Laboratories, Albuquerque, NM, Sandia Report SAND2006-7729, Unlimited Release, 2006.

[8] Bayindir, C.
Enhancements to synthetic aperture radar chirp waveforms and non-coherent SAR change detection following large scale disasters.
Ph.D. thesis, *School of Electrical and Computer Engineering, Georgia Institute of Technology*, Atlanta, GA, 2013.

[9] Cumming, I. G., Neo, Y. L., and Wong, F.
Interpretations of the omega-K algorithm and comparisons with other algorithms.
In *Proceedings of the IEEE International Geoscience and Remote Sensing Symposium*, **3**, Toulouse, France, 2003, 1455–1458.

[10] Carrara, W. G., Goodman, R. S., and Majewski, R. M.
Spotlight Synthetic Aperture Radar: Signal Processing Algorithms. Norwood, MA: Artech House, 1995.

[11] Soumekh, M.
Synthetic Aperture Radar Signal Processing with MATLAB Algorithms. New York: John Wiley & Sons, Inc., 1999.

[12] Cook, E.
A class of nonlinear FM pulse compression signals.
Proceedings of the IEEE, **52**, 11 (1964), 1369–1371.

[13] Levanon, N., and Mozeson, E.
Radar Signals. Hoboken, NJ: Wiley, 2004.

[14] Brandon, P. S.
The design of a nonlinear pulse compression system to give a low loss high resolution radar performance.
Marconi Review, **36**, 188 (1973), 1–45.

[15] Price, R.
Chebyshev low pulse compression sidelobes via a nonlinear FM.
In *National Radio Science Meeting of URSI*, Seattle, WA, 1979.

[16] Yichun, P., Shirui, P., Kefeng, Y., and Wenfeng, D.
Optimization design of NLFM signal and its pulse compression simulation.
In *Proceedings of the IEEE Radar Conference*, Arlington, VA, May 2005, 383–386.

[17] Gembicki, F. W., and Haimes, Y. Y.
Approach to performance and sensitivity multiobjective optimization: The goal attainment method.
IEEE Transactions on Automatic Control, **20**, 6 (1975), 769–771.

[18] Cumming, I. G., and Wong, F. H.
Digital Processing of Synthetic Aperture Radar Data Algorithms and Implementation. Norwood, MA: Artech House, 2005.

[19] Junjie, W., Zhongyu, L., Yulin, H., Jianyu, Y., and Qing, H. L.
Omega-K imaging algorithm for one-stationary bistatic SAR.
IEEE Transactions on Aerospace and Electronic Systems, **50**, 1 (2014), 33–52.

[20] Fornaro, G.
Trajectory deviations in airborne SAR: Analysis and compensation.
IEEE Transactions on Aerospace and Electronic Systems, **35**, 3 (1999), 997–1009.

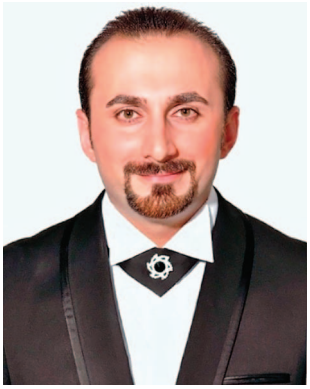

Jamal Saeedi was born in Amol, Iran, in 1984. He received the B.Sc. degree in biomedical engineering from Sahand University of Tabriz, Iran, in 2007, and his M.Sc. and Ph.D. degrees in electronic engineering from Amirkabir University of Tehran, Iran, in 2010 and 2015, respectively. He works in the field of signal and image processing, specializing particularly in information fusion, pattern recognition, radar systems design, radar jamming and deception, and synthetic aperture radar imaging. He has over 18 publications in various areas, including signal and image processing, radar, and synthetic aperture radar.

Karim Faez was born in Semnan, Iran. He received his B.S. degree in electrical engineering from Tehran Polytechnic University as the first rank in June 1973, and his M.S. and Ph.D. degrees in computer science from the University of California at Los Angeles (UCLA) in 1977 and 1980, respectively. Professor Faez was with the Iran Telecommunication Research Center (1981–1983) before joining Amirkabir University of Technology (Tehran Polytechnic) in Iran, where he is now a professor of electrical engineering. He was the founder of the Computer Engineering Department of Amirkabir University in 1989, and he served as its first chairman during April 1989–September 1992. His research interests are in pattern recognition, image processing, neural networks, signal processing, Farsi handwritten processing, earthquake signal processing, fault tolerant system design, computer networks, and hardware design. He is a member of Institute of Electrical and Electronics Engineers, Institute of Electronics, Information and Communication Engineers, and Association for Computing Machinery.